Anisotropic transport in the quasi-one-dimensional semiconductor $Li_{0.33}MoO_3$

S. Moshfeghyeganeh,[1] A. N. Cote,[1,a)] J. J. Neumeier,[2] and J. L. Cohn[1,b)]
[1]*Department of Physics, University of Miami, Coral Gables, Florida 33124, USA*
[2]*Department of Physics, Montana State University, Bozeman, Montana 59717, USA*

(Received 9 December 2015; accepted 18 February 2016; published online 4 March 2016)

Transport measurements (electrical resistivity, Seebeck coefficient, and thermal conductivity) in the temperature range 80–500 K are presented for single crystals of the quasi-one-dimensional (Q1D) semiconductor $Li_{0.33}MoO_3$. Opposite signs are observed for the Seebeck coefficient along the trinclinic a and c axes, with $S_c - S_a \simeq 250\,\mu$V/K near room temperature and $\simeq 100\,\mu$V/K at 380 K. The thermal conductivity at room temperature in the a-c planes was $\sim$2 W/m K and $\sim$10 times smaller along b^*. A weak structural anomaly at $T_s \approx 355$ K, identified in the temperature-dependent lattice constants, coincides with anomalies in the electrical properties. Analysis of the electronic transport at $T > T_s$ favors an intrinsic semiconductor picture for transport along the most conducting Q1D axis and small-polaronic transport along the other directions, providing insight into the origin of the Seebeck anisotropy. © *2016 AIP Publishing LLC*.
[http://dx.doi.org/10.1063/1.4943071]

I. INTRODUCTION

Bulk materials with highly anisotropic Seebeck coefficients are potential candidates for transverse thermoelectric applications[1,2] but are quite rare. The molybdenum oxide bronzes[3] are a class of low-dimensional materials that have potential as anisotropic thermoelectrics. Recently, we reported that the quasi-one-dimensional (Q1D) metal, $Li_{0.9}Mo_6O_{17}$ (lithium purple bronze), has extreme anisotropy in its Seebeck coefficient along mutually perpendicular crystallographic axes ($\sim$200 μV/K) and exhibits among the largest known transverse thermoelectric figures of merit of any bulk material.[4] A closely related Q1D compound which we discuss here is $Li_{0.33}MoO_3$. Like lithium purple bronze, it was first synthesized in the 1980s,[5–7] but transport studies, showing it to be a narrow-gap semiconductor, were limited to resistivity along two of the main symmetry directions.

$Li_{0.33}MoO_3$ is unique among Mo bronzes in possessing a triclinic structure (Fig. 1), with lattice constants[7] $a = 13.079$ Å, $b = 15.453$ Å, and $c = 7.476$ Å, and angles, $\alpha = 96.97°$, $\beta = 106.56°$, and $\gamma = 103.368°$. The most conducting c axis is characterized by infinite chains of corner-sharing MoO_6 octahedra with good Mo-O-Mo $d_{t_{2g}}$–$p\pi$ orbital overlap associated with Mo-O bondlengths, 1.86–1.995 Å. The direction transverse to the a-c planes (designated b^*) is characterized by both corner- and edge-sharing MoO_6 octahedra, with some Mo-O distances as large as 2.7 Å and thus much poorer overlap. Tight binding band calculations[9] indicate that $Li_{0.33}MoO_3$ is a small-gap semiconductor ($E_g \approx 0.10$ eV), in reasonable agreement with resistivity measurements.[10] This prior work[10] identified a change in the c-axis resistivity temperature dependence near 360 K, suggestive of a broad phase transition; differential scanning calorimetry and powder x-ray diffraction showed no signature of this transition. Our measurements show the Seebeck coefficient along the most conducting c axis to be particularly sensitive to this transition, and we present temperature-dependent, single-crystal x-ray diffraction studies which reveal a weak structural anomaly upon cooling through $T_s \approx 355$ K. $Li_{0.33}MoO_3$ is found to be a rare $p \times n$-type material,[2] having opposite signs for the Seebeck coefficient

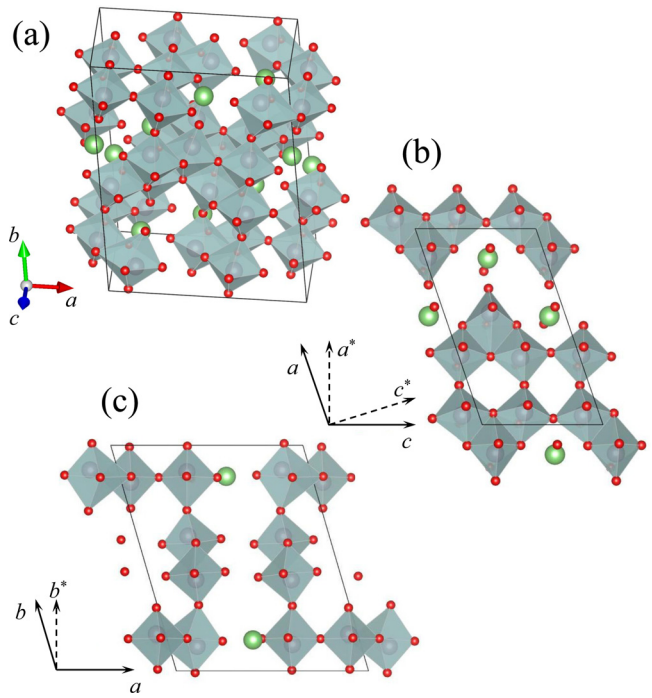

FIG. 1. (a) The triclinic unit cell of $Li_{0.33}MoO_3$. Conduction pathways consist of edge- and corner-sharing MoO_6 octahedra (shaded). Projections of a single atomic layer are shown within the (b) ac-plane viewed along the b axis and (c) ab-plane viewed along the c axis. The c-axis corresponds to the most conducting (Q1D) direction. Rendered with VESTA software (Ref. 8).

a)Present address: Department of Physics, University of Illinois at Urbana-Champaign, Urbana, Illinois 61801-3080, USA.
b)Electronic mail: cohn@physics.miami.edu

along the crystal axes of the *a*-*c* planes in the entire temperature range explored, leading to extreme anisotropy, $S_c - S_a \simeq 250\,\mu$V/K at 300 K. Even at $T > T_s$, the Seebeck anisotropy remains quite large, $S_c - S_a \simeq 100\,\mu$V/K at 380 K. The origin of this anisotropy is examined by analyzing the data with both intrinsic semiconductor and small-polaron models.

II. EXPERIMENT

Single crystals were grown using the temperature-gradient flux method.[6,11] Li_2MoO_4, MoO_3, and MoO_2 were mixed according to the formula $nLi_2MoO_4 + 2(1-n)MoO_3 + nMoO_2 \rightarrow 2Li_nMoO_3$, with $n = 0.26$. The crystal charge had a total mass of 10 g. It was placed in a fused silica tube with inside diameter 1.2 cm and length 16 cm on Pt foil to minimize reaction with the silica. The tube was evacuated for 4 h and sealed under a vacuum of 1.4×10^{-2} mbar. It was placed in a furnace and warmed over a period of 2 h to the maximum temperature where it remained for 124 h, such that one end of the tube was at 586 °C and the other at 632 °C. Subsequently, it was cooled over a period of 2 h to room temperature. Crystals of $Li_{0.33}MoO_3$ were mechanically removed from the flux.

Precision lattice constants were determined by high-angle extrapolation[12] of the (*h*00), (0*k*0), and (00*l*) reflections (with error bars $\lesssim \pm 0.0007$ Å). Specimens for transport measurements were cut with a wire saw into parallelepipeds with typical dimensions, $1.5 \times 0.5 \times 0.2\,\text{mm}^3$. Electrical contacts for four-wire measurements employed silver epoxy, annealed at 330 °C for 1 h, and 25 μm-diameter Au wires. Current contacts covered the specimen ends, and voltage contacts encircled the crystal across both large faces and the sides. Thermopower and thermal conductivity measurements employed a steady-state method using a small chip heater and 25 μm differential chromel-constantan thermocouple, each attached to the specimen with epoxy (Stycast 2850 FT). The temperature of the Cu heat sink was measured using a platinum sensor. Heat losses due to radiation and conduction through lead wires were determined in separate experiments; these corrections were 20%–30% near room temperature. The accuracy of the measurements is limited by uncertainty in the geometric factor to 20%. The measurements were performed on three crystals each along the *a* and *c* directions, and for two crystals along the *b** direction; good reproducibility was observed.

III. RESULTS

A. Transport coefficients

Figure 2 shows the temperature-dependent electrical resistivity (ρ) and the Seebeck coefficient (S) along three crystallographic axes for several $Li_{0.33}MoO_3$ crystals. The electronic transition near 355 K is clearly seen in the *c*-axis resistivity and Seebeck data and is accentuated in the logarithmic temperature derivative of ρ_c (inset, Fig. 2). The present crystals have values for ρ_c that are a factor of 10 larger than those reported by Collins *et al.*[10] The reproducibility of this result in three separate crystals with differing thicknesses and aspect ratios makes it unlikely to be attributable to "contamination" by contributions from the other transport

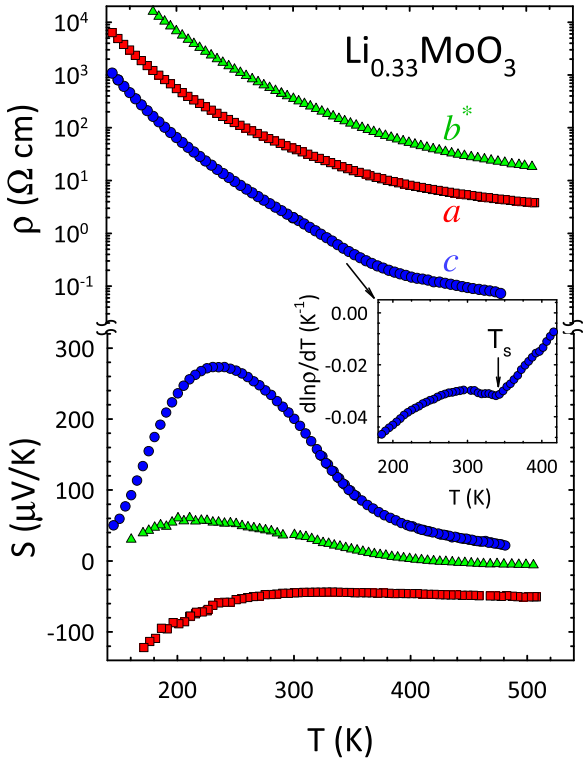

FIG. 2. Resistivity and Seebeck coefficient of $Li_{0.33}MoO_3$ crystals in the range of 200–500 K for three crystallographic directions. Inset: Logarithmic temperature derivative of ρ_c highlighting the transition at $T_s \simeq 355$ K.

directions due to inhomogeneous current flow. The difference is possibly extrinsic, i.e., associated with different doping levels. The resistivity ratios of the present crystals are $\rho_c : \rho_a : \rho_{b^*} \simeq 1 : 20 : 180$ at 300 K and 1:50:330 at 375 K, and thus $Li_{0.33}MoO_3$ is appropriately categorized as a Q1D semiconductor. Particularly noteworthy for potential transverse thermoelectric applications is the opposite sign for the *a*- and *c*-axis Seebeck coefficients, yielding extreme anisotropy, $\Delta S = S_c - S_a \simeq 250\,\mu$V/K at 300 K.

The thermal conductivity (κ) is quite low for all directions (Fig. 3), ~2 W/m K within the *a*-*c* plane at room temperature and about 10 times smaller along *b**. The Wiedemann-Franz law and the electrical resistivity imply a negligible electronic contribution to κ, and thus the data in Fig. 3 reflect the anisotropy of lattice conduction. We expect relatively little anisotropy within the *a*-*c* planes, consistent with observations. The anisotropy ratio $\kappa_{ac}/\kappa_{b^*} \sim 10$ is typical of layered insulators and low-carrier density materials (e.g., mica and graphite).[13,14]

B. Structural anomaly near T = 355 K

A structural signature of the electronic transition, not established in prior work,[10] is revealed at $T_s \approx 355$ K in the lattice constant temperature dependencies (Fig. 4). Upon cooling through T_s, the data show a slight lattice contraction (by ≃0.001 Å) along the *a** direction, and expansions comparable in magnitude along *b** and *c** (for *c**, this is an upper bound given additional scatter). Most noteworthy is the opposite sign and substantially smaller magnitude of the temperature derivative of the *c** lattice constant as compared

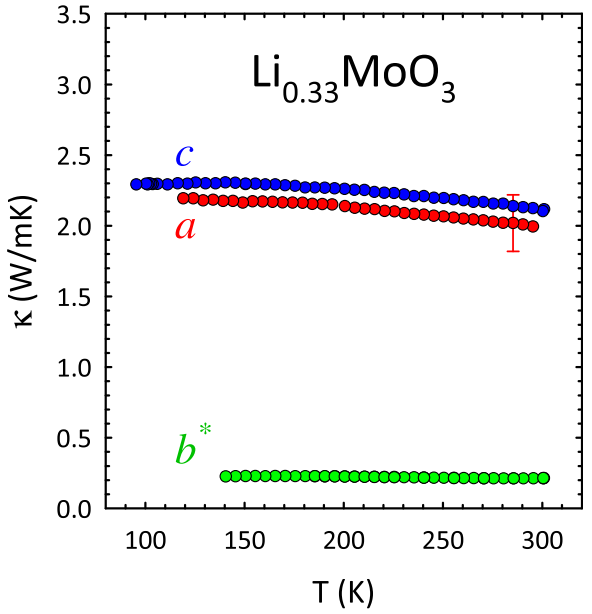

FIG. 3. Thermal conductivity of $Li_{0.33}MoO_3$ single crystals along different crystallographic axes. The error bar reflects a 20% uncertainty in the geometric factor.

to those for the other two directions (solid lines and labels). The structural feature at T_s likely involves a subtle rearrangement of the tilt pattern and/or distortion of some of the MoO_6 octahedra.

IV. ANALYSIS AND DISCUSSION

We focus our analysis on the regime $T > T_s = 355\,\mathrm{K}$ where the charge transport exhibits a simple thermally activated behavior (shown in Fig. 5 for c-axis transport). A key observation for assessing the transport mechanism is that the characteristic activation energy for the resistivity exceeds that of the thermopower for all transport directions. This dictates consideration of two transport models: (1) intrinsic band semiconductor and (2) small-polaron. For an intrinsic semiconductor[15]

$$\rho = \rho_0 \exp\left(E_g/2k_BT\right),$$
$$S = -\frac{k_B}{|e|}\frac{\beta-1}{\beta+1}\left(\frac{E_{g0}}{2k_BT} + 2 + \frac{\gamma}{2k_B}\right), \tag{1}$$

where $E_g = E_{g0} + \gamma T$ is the temperature-dependent energy gap (approximated as linear-in-T), and $\beta = \mu_e/\mu_h$ is the electron/hole mobility ratio. The constant term, 2, in the parentheses of the thermopower expression assumes predominant acoustic-mode lattice scattering of the carriers.

In contrast, ρ and S for small polarons are given by[16,17]

$$\rho = \frac{\hbar a}{c(1-c)e^2}\left(\frac{T}{T_0}\right)^s \exp\left(E_\rho/k_BT\right),$$
$$S = \frac{k_B}{|e|}\left[\frac{E_S}{k_BT} - \ln\frac{c(1-c)}{(1-2c)^2}\right], \tag{2}$$

where a is the hopping distance, c is the polaron concentration, and T_0 is an energy scale that depends on whether the

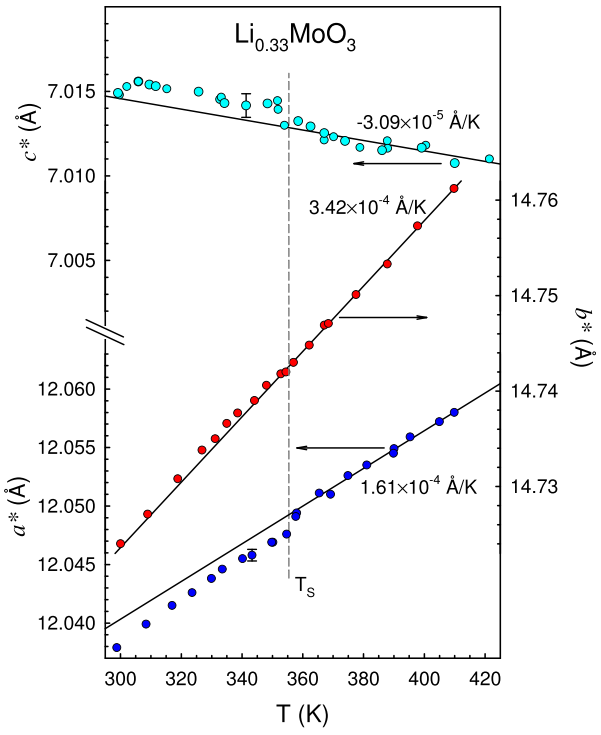

FIG. 4. Lattice constants *vs.* T for single-crystal $Li_{0.33}MoO_3$. The error bars for a^* and b^* are ± 0.0005 Å and ± 0.0007 Å for c^*. The solid lines are linear least-squares fits to the data for $T \geq T_s \simeq 355\,\mathrm{K}$.

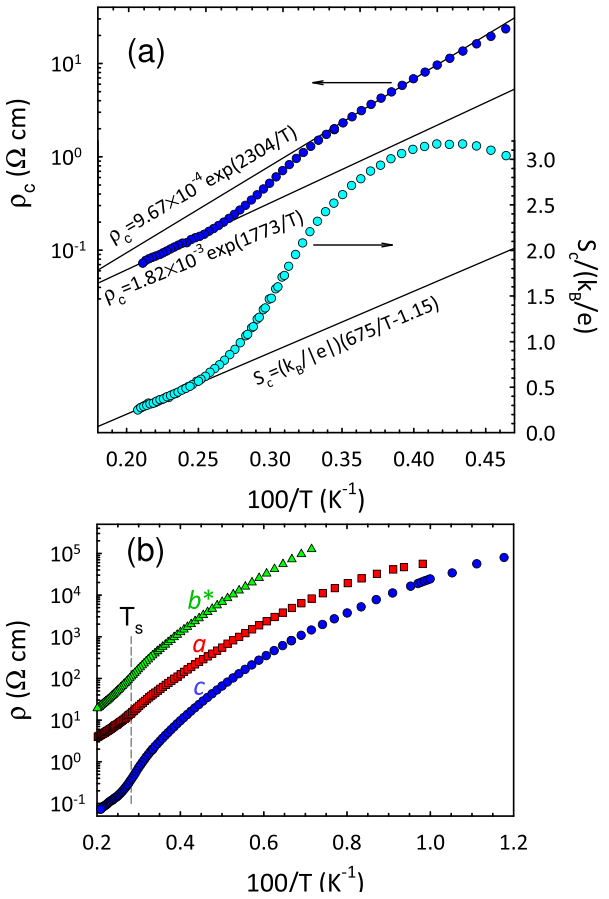

FIG. 5. (a) ρ_c and S_c plotted against inverse temperature, showing thermally activated behavior near $T_s \simeq 355\,\mathrm{K}$. The solid lines are linear least-squares fits. (b) Resistivity data for all directions, extended to lower T.

electronic motion is faster than that of the lattice (adiabatic limit, $s=1$) or not (non-adiabatic, $s=3/2$). In the adiabatic limit, $k_BT_0=\hbar\omega_0$, where $\omega_0\sim10^{14}\,s^{-1}$ is an optical phonon frequency. The condition for non-adiabatic behavior is $k_BT_0\ll\hbar\omega_0$. Using the experimental data, discussed further below, we find $k_BT_0\ll\hbar\omega_0$, thus favoring the non-adiabatic limit. Within small-polaron theory, $E_\rho\gg E_S$ because E_S includes only the energy required to thermally excite a charge carrier from the Fermi level to the polaron band, whereas E_ρ includes, in addition, the lattice distortion energy.

We first fit the data at $T>T_s$ to the intrinsic semiconductor model, Eq. (1). The results for the c-axis transport are shown in Fig. 5(a) and imply $E_{g0}/k_B=3550\,K$ ($E_{g0}\simeq0.31\,eV$), $\gamma=-0.88\,meV/K$, and $\beta\simeq0.45$, i.e., the hole mobility is about twice that of electrons. This value of E_{g0} is somewhat larger than predicted from tight-binding band calculations,[9] which considered only the infinite chains of MoO_6 octahedra along the c axis relevant to d_{xy} bands dispersing along the Γ–Z direction of the Brillouin zone. In the temperature regime just below T_s, the fitting of $\rho_c(T)$ yields $E_{g0}/k_B\simeq4610\,K$ ($E_{g0}\simeq0.40\,eV$), i.e., the structural transition increases the energy gap by about 30%. The parameters from similar analyses of the a- and b^*-axis data are summarized in Table I. At lower temperatures [Fig. 5(b)], the $\rho(T)$ data for all directions become weakly T-dependent, indicating impurity conduction (along c) or small-polaron band conduction (along a and b^*—see below). Supporting this, the maxima and subsequent decline in the magnitudes of S_c and S_{b^*} at $T\lesssim200\,K$ suggest a finite density of states at E_F as $T\to0$.

The values for $\gamma\equiv dE_g/dT$ are larger than for typical semiconductors,[18,19] by a plausible factor of two for the c axis, but appear to be unphysically large for the a and b^* directions. This is a consequence of the larger values of β required within the model to produce the much smaller thermopower activation energies for these crystallographic directions. In fact, the $T\to\infty$ intercepts of the thermopower (negative for all directions) do not differ substantially in magnitude (varying from -1.2 to -0.36 in k_B/e units), thus the Seebeck anisotropy in the measured temperature range is largely attributable to these smaller activation energies, and thus motivates consideration of the small-polaron model.

The parameters from fitting the electronic transport data to the non-adiabatic, small-polaron model [Eq. (2)] are listed in Table II. In computing T_0, we assume a value for the hopping distance $a=5\,Å$, i.e., an average of the Mo-Mo nearest-neighbor and next-nearest-neighbor distances. For completeness, we include the parameters for the c axis in Table II, but it is clear that such an analysis is not self consistent. Our analysis thus favors an intrinsic semiconductor picture for the electronic transport along the Q1D (c) axis and transport via non-adiabatic small polarons along the other crystallographic directions.

TABLE I. Energy gap, resistivity prefactor (ρ_0), electron/hole mobility ratio (β), and energy gap linear temperature coefficient (γ), determined from fits to the $T>T_s$ $\rho(T)$ and $S(T)$ data using the intrinsic semiconductor model, Eq. (1).

Axis	E_{g0} (eV)	$\rho_0(m\Omega\,cm)$	β	γ(meV/K)
c	0.31	1.82	0.45	−0.88
a	0.25	214	0.87	−2.28
b^*	0.33	411	0.86	−1.16

TABLE II. Activation energies and other parameters from fits to the $T>T_s$ $\rho(T)$ and $S(T)$ data using the non-adiabatic small-polaron model, Eq. (2). The values for T_0 assume a hopping length $a=5\,Å$.

Axis	E_ρ (eV)	E_S (meV)	ρ_0 ($\mu\Omega$ cm/K$^{3/2}$)	c	T_0 (K)
c	0.210	59.1	4.35×10^{-2}	0.634	0.075
a	0.183	8.50	4.97	0.660	32.4
b^*	0.224	12.6	9.31	0.693	22.1

In summary, the Q1D semiconductor $Li_{0.33}MoO_3$ is a $p\times n$-type thermoelectric material with large Seebeck anisotropy within its triclinic a-c planes. A weak structural anomaly, coincident with changes in the electronic transport at 355 K, was identified by small changes in the lattice parameters (~0.001 Å). Analysis of the transport at temperatures above the transition suggests that an intrinsic semiconductor picture for transport along the most conducting c axis is appropriate, with a hole mobility about twice that of electrons. Along the a and b^* directions, a non-adiabatic small-polaron model was found to be a better description of the data. This dichotomy of transport mechanisms appears to be responsible for the substantially different thermopower activation energies characterizing the transport along the Q1D c axis as compared to the other crystallographic directions and is the origin of the Seebeck anisotropy.

ACKNOWLEDGMENTS

This material is based upon work supported by the U.S. Department of Energy (DOE)/Basic Energy Sciences (BES) Grant No. DE-FG02-12ER46888 (Univ. Miami) and the National Science Foundation under Grant No. DMR-0907036 (Mont. St. Univ.).

[1]C. Reitmaier, F. Walther, and H. Lengfellner, Appl. Phys. A **99**, 717 (2010).
[2]C. Zhou, S. Birner, Y. Tang, K. Heinselman, and M. Grayson, Phys. Rev. Lett. **110**, 227701 (2013).
[3]M. Greenblatt, Chem. Rev. **88**, 31 (1988).
[4]J. L. Cohn, S. Moshfeghyeganeh, C. A. M. dos Santos, and J. J. Neumeier, Phys. Rev. Lett. **112**, 186602 (2014).
[5]P. Strobel and M. Greenblatt, J. Solid State Chem. **36**, 331 (1981).
[6]W. H. McCarroll and M. Greenblatt, J. Solid State Chem. **54**, 282 (1984).
[7]P. P. Tsai, J. A. Potenza, M. Greenblatt, and H. J. Schugar, J. Solid State Chem. **64**, 47 (1986).
[8]K. Momma and F. Izumi, J. Appl. Crystallogr. **44**, 1272 (2011).
[9]E. Canadell and M.-H. Whangbo, Inorg. Chem. **27**, 228 (1988).
[10]B. T. Collins, K. V. Ramanujachary, and M. Greenblatt, J. Solid State Chem. **76**, 319 (1988).
[11]C. A. M. dos Santos, B. D. White, Y.-K. Yu, J. J. Neumeier, and J. A. Soza, Phys. Rev. Lett. **98**, 266405 (2007).
[12]B. D. Cullity, *Elements of X-ray Diffraction*, 3rd ed. (Addison-Wesley, 2001).
[13]A. S. Gray and C. Uher, J. Mater. Sci. **12**, 959 (1977); W.-P. Hsieh, B. Chen, J. Li, P. Keblinski, and D. G. Cahill, Phys. Rev. B **80**, 180302(R) (2009).
[14]G. A. Slack, Phys. Rev. **127**, 694 (1962); C. A. Klein and M. G. Holland, *ibid.* **136**, A575 (1964).

[15]V. A. Johnson and K. Lark-Horovitz, Phys. Rev. **92**, 226 (1953).
[16]D. Emin, in *Electronic Structure Properties of Amorphous Semiconductors*, edited by P. G. Le Comber and N. F. Mott (Academic Press, New York, 1973). See also M. S. Hillery, D. Emin, and N.-L. H. Liu Phys. Rev. B **38**, 9771 (1988).
[17]M. Jaime, M. B. Salamon, M. Rubinstein, R. E. Treece, J. S. Horwitz, and D. B. Chrisey, Phys. Rev. B **54**, 11914 (1996).
[18]Y. P. Varshni, Physica **34**, 149 (1967).
[19]J. Bhosale, A. K. Ramdas, A. Burger, A. Muñoz, A. H. Romero, M. Cardona, R. Lauck, and R. K. Kremer, Phys. Rev. B **86**, 195208 (2012).